

pubs.acs.org/Biomac Article

Dual Biochemically Breakable Drug Carriers from Programmed Telechelic Homopolymers

Adrian Moreno,* Ana Jiménez-Alesanco, Juan C. Ronda, Virginia Cádiz, Marina Galià, Virgil Percec, Olga Abian, and Gerard Lligadas*



Cite This: *Biomacromolecules* 2020, 21, 4313–4325



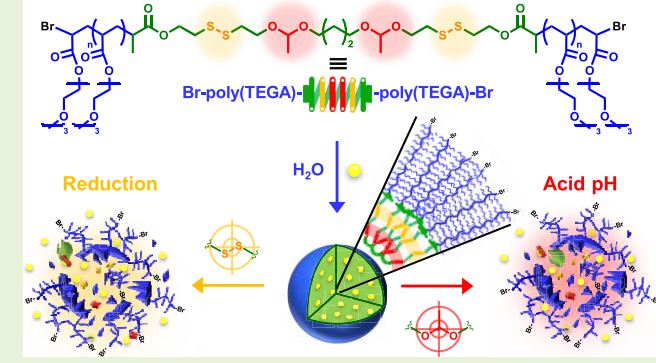
ACCESS

III Metrics & More

Article Recommendations

si Supporting Information

ABSTRACT: Well-defined hydrophilic telechelic dibromo poly-(triethylene glycol monomethyl ether acrylate)s were prepared by single-electron transfer living radical polymerization employing a hydrophobic difunctional initiator containing acetal and disulfide linkages. Although the resulting homopolymers have low hydrophobic contents (<8.5 wt % of the entire structure), they are able to self-assemble in water into nanoscale micellelike particles via chain folding. Acetal and disulfide linkages were demonstrated to be "keystone" units for their dual stimuli-responsive behavior under biochemically relevant conditions. Their site-selective middle-chain cleavage under both acidic pH and reductive conditions splits the homopolymer into two equal-sized fragments and results in the breakdown of the nanoassemblies. The drug loading/delivery



potential of these nanoparticles was investigated using curcumine combining in vitro drug release, cytotoxicity, and cellular uptake studies with human cancer cell lines (HT-29 and HeLa). Importantly, this strategy may be extended to prepare innovative nanoplatforms based on hydrophilic homopolymers or random copolymers for intelligent drug delivery.

■ INTRODUCTION

Amphiphilic polymer design represents a captivating class of biorelevant templates on account of their ability to form a range of different nanoassemblies such as spherical micelles, vesicles, and cylinders in aqueous media. 1-5 Although most of these selforganized structures rely on block copolymers, the self-directed assembly of amphiphilic homopolymers represents a promising direction to give rise to high-order morphologies in solution, greatly benefiting from the common easier synthetic accessibility of their precursors.^{6,7} Making the most of the key advances in controlled/living polymerization methods, associative homopolymers are classically based on amphiphilically equipped monomers (Scheme 1A)⁸⁻¹² or alternatively consist of welldefined fully hydrophilic homopolymers with one or two hydrophobic end group(s) (Scheme 1B). 13-17 Mimicking conventional amphiphilic block copolymers, their homopolymer analogues can also form micellar, 18,19 vesicular, 20,21 and related aggregates in water as well as reverse structures in nonpolar solvents. 22,23

Meanwhile, over the past several years, interest in gaining precise control over solution-state self-assembled polymer morphologies has exploded, leading to a huge variety of macromolecular architectures that enable stimuli-induced morphological changes, e.g., volume expansion, or transitions, e.g., micelles to vesicles. ^{5,24–26} In this regard, for many biological applications, e.g., drug delivery and imaging, the development of

nanoassemblies, which are designed to undergo complete breakdown and release cargo(s) in response to external stimuli, is highly desirable and represent an ultimate goal. Acidic pH, temperature, light, and redox potential, among others, are typical stimuli that have been extensively explored. However, dual or multistimuli-breakable systems are even more advantageous to make the release process more efficient, accurate, and controllable.

Previously, we have shown that fully hydrophilic telechelic dibromopolymers prepared by combining single-electron transfer living radical polymerization (SET-LRP)^{36–38} with hydrophobic diffunctional initiators (DIs) are a convenient means of synthesizing associative telechelic homo or random polymers with predicted molecular weight, narrow polydispersity, and high chain-end functionality (Scheme 1C).^{39,40} The aqueous self-assembly of these amphiphilic homopolymers results in initiator residue incorporation at the hydrophobic core of micelle-like nanoassemblies via chain folding. This amphiphilic homopolymer design is especially attractive in terms of control

Received: July 23, 2020 Revised: September 4, 2020 Published: September 8, 2020

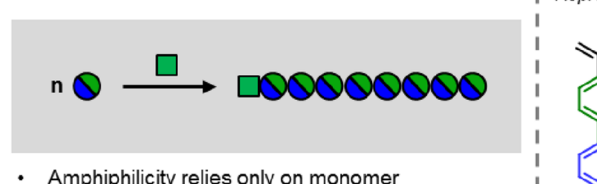




Biomacromolecules Article pubs.acs.org/Biomac

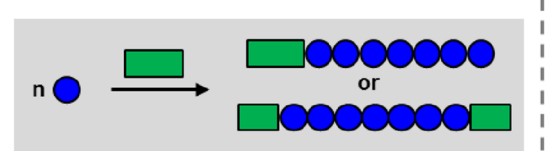
Scheme 1. Schematic Representation of the Synthetic Pathways to Amphiphilic Homopolymers

A Previous works: amphiphilic homopolymers based on amphiphilic monomers



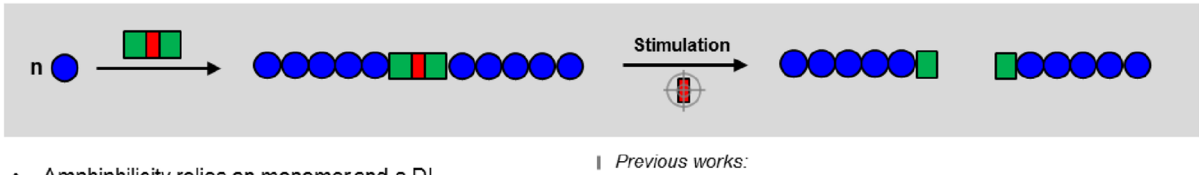
- Amphiphilicity relies only on monomer
- Most examples use ATRP
- Polymer design also accessible by postpolymerization modification approach^{18,19,23}

B Previous works: amphiphilic homopolymers based on fully hydrophilic chains with hydrophobic end group(s)



- Amphiphilicity relies on monomer and monofunctional initiator/chain transfer agent.
- Most examples use RAFT polymerization
- Possibility to use commercial hydrophilic monomers

C Our design: amphiphilic homopolymers based on fully hydrophilic telechelic chains with hydrophobic middle core



- Amphiphilicity relies on monomer and a DI
- Possibility to integrate middle-chain degradability using stimulicleavable DIs
- The use of SET-LRP ensures high chain end fidelity which is crucial for certain applications 39
- Possibility to use commercial hydrophilic monomers

"Color code: blue, hydrophilic and water-soluble; green, hydrophobic and water-insoluble; and red, stimuli-cleavable linkages.

over the disassembly process because the chemical engineering of DI enables the programming of a predetermined degradation code by introducing labile linkages into its design. The use of hydrophobic DIs containing cleavable functions enables the reduction of the number-average molar mass (M_n) by half after degradation, which dramatically modifies the amphiphilic balance (Scheme 1C), 41,42 further resulting in the breakdown of the nanoassemblies. 39,40

Herein, we report a facile strategy to prepare dual pH and reduction-breakable micelle-like nanoassemblies, formed from the self-directed assembly of fully hydrophilic poly(triethylene glycol monomethyl ether acrylate)s [poly(TEGA)s] prepared via SET-LRP employing a hydrophobic DI integrating acetal and disulfide cleavable linkages as double dual "keystone" units. Although dual acidic pH/reduction-responsive degradable block copolymer systems have received increasing attention for cellular delivery applications by means of increased acidity and glutathione (thiol) concentration of tumor cells or tissues compared to the healthy ones, 35,43-45 this is the first example of homopolymers that act in the same way as amphiphilic block copolymers. Despite containing a low hydrophobic fraction of the hydrophobic initiator residue (<8.5 wt %), the synthesized homopolymers were able to self-assemble in aqueous solution and encapsulate hydrophobes into their core. We vividly demonstrated the dual capability of the conceived assemblies to swell and finally breakdown under biochemically relevant conditions, i.e., weakly acidic and/or reductive environments, owing to the site-selective middle-chain cleavage of acetal and/ or disulfide units. Additionally, the potential of these amphiphilic homopolymers for effective loading and delivering of anticancer drugs has been tested using curcumine (CC) as a model hydrophobic drug.

■ EXPERIMENTAL SECTION

TEGA Monomer Synthesis. Triethylene glycol monomethyl ether (25 g, 0.15 mol) and anhydrous TEA (31 mL, 0.20 mol) were dissolved in anhydrous Me-THF (60 mL) under a positive flow of argon. Then, the solution was placed in an ice bath (0–5 $^{\circ}C)$ and allowed to stir for 30 min before starting the addition of acryloyl chloride (18 mL, 0.22 mol) dissolved in Me-THF (20 mL). The reaction was then allowed to

proceed for 24 h at room temperature. After this, the crude mixture was filtered and the excess of Me-THF was removed under reduced pressure. The final residue was purified by vacuum distillation, in the presence of 5 (w/w%) of hydroquinone, to afford TEGA (23.6 g, 83%) as a colorless viscous liquid. ¹H NMR analysis was consistent with previous reports. ⁴⁶

General Procedure for SET-LRP. This procedure is representative for all of the polymerizations conducted herein. The SET-LRP of TEGA using DI_{A/R} as an initiator in DMSO under the following conditions $[TEGA]_0/[DI_{A/R}]_0/[Me_6-TREN]_0 = 50/1/0.2$ is described. The initiator DI_{A/R} (34 mg, 1 mmol) was dissolved in DMSO (0.25 mL) and charged in a 25 mL Schlenk flask together with the TEGA monomer (0.5 mL, 2.3 mmol) and the Me₆-TREN ligand (2.6 μ L, 0.2 mmol). Next, the oxygen was removed from the reaction mixture by six consecutive freeze-pump (1 min)-thaw (F-P-T) cycles. After this, a piece of surface-activated copper wire (4.5 cm), coil wrapped around a Teflon-coated magnetic stir bar, was introduced into the flask under a strong flow of argon and held above the reaction mixture using an external neodymium magnet. Two F-P-T cycles were applied, and after this, the reaction mixture was placed in a thermostat bath at 25 °C. The introduction of the magnetic stir bar into the reaction vessel started the polymerization process (t = 0). In general, the reactions were allowed to proceed for 2 h, and only for kinetic experiments, monomer conversion was determined by periodic withdrawing of samples at different times through the side arm of the tube previously purged with argon using a Hamilton gastight syringe. The collected samples were dissolved and analyzed by ¹H NMR to determine the monomer conversion followed by solvent evaporation to determine the molecular weight by GPC. The final polymer was purified before any further studies by passing the diluted (THF) crude solution through a short basic alumina column to remove copper salt residues and subsequently by dialysis against acetone (yield 85-89%). Poly(triethylene glycol monomethyl ether acrylate) (ATHs): ¹H NMR (400 MHz, CDCl₂, δ) = 4.7 (q, 2H), 4.34-4.15 (m, 6H), 3.8 (dd, 4H), 3.6-3.5 (m, 8H), 3.4(s, 6H), 2.8 (m, 4H), 2.5-1.5 (m, 18H), 1.35 (d, 6H), 1.13 (m, 6H); ¹³C NMR (100.6 MHz, CDCl₃, δ) = 170.04, 160.98, 99.83, 70.55, 65.34, 63.71, 63.06, 61.89, 52.65, 39.79, 39.27, 36.64, 32.45, 26.69, 21.62, 19.68,

General Procedure to Conduct Middle-Chain Cleavage of Amphiphilic Telechelic Homopolymers (ATHs). A solution of ATH (50 mg) in THF (2 mL) was introduced into a 5 mL round-bottomed flask equipped with a magnetic stir bar. After this, TFA (80 μ L, 0.1 M in THF), for acid cleavage, or PBu $_3$ (200 μ L, 100 equiv), for reductive cleavage, was added, and the resulting reaction mixture was allowed to stir during 1 h at room temperature under an argon atmosphere. The reaction mixture was passed through a short basic alumina column prior to GPC analysis.

Self-Assembly of ATHs and CC Loading. ATH nanoassemblies were prepared by two different procedures: nanoprecipitation (solventswitch method) and direct dispersion in water. The nanoprecipitation method was conducted as follows. First, 10 mg of ATH was dissolved in 1 mL of THF. To this solution, 7 mL of Milli Q water was added progressively at a rate of 15 μ L·min⁻¹ in a total of 7 h using a syringe pump from Thermo Fisher Scientific. The excess of THF was removed by dialysis against PBS (pH = 7.4) during 1 day using a dialysis membrane with an MWCO of 2000 kDa. The final mixture was diluted to 10 mL using a phosphate buffer solution to reach a final concentration of 1 mg \cdot mL⁻¹. Self-assembly by direct dispersion was conducted by simply mixing ATH and water at 1 mg·mL⁻¹. The preparation of CC-loaded nanoassemblies was conducted as follows: ATH (10 mg) and CC (1.2 mg) were dissolved in THF (1 mL), and Milli Q water was progressively added to the organic solution following the above-described nanoprecipitation methodology. After this, the unencapsulated CC was removed by filtering the solution through a nylon membrane (0.45 μ m). The drug-loading content (DLC) and encapsulation efficiency (EE) values were determined by freeze drying the CC-loaded nanoassembly solution followed by redispersion in acetone and analysis by fluorescence emission spectra at 517 nm using a standard calibration curve. The DLC and EE values were calculated according to the following equation: DLC (%) = (weight of drug loaded

in nanoassemblies)/(weight of nanoassemblies) \times 100, and EE (%) = (amount of loaded drug)/(total amount of feeding drug) \times 100.

Determination of Critical Aggregation Concentration (CAC). The CAC was determined using NR as a fluorescent probe by direct monitoring of the emission changes with a peak at 617 nm. Fluorescence emission spectra were recorded by fixing the excitation wavelength at 550 nm at an emission range of 560-720 nm. The concentration of AHPs was varied from 1.0×10^{-9} to $1.0 \text{ mg} \cdot \text{mL}^{-1}$, and the NR concentration was fixed at 6.7×10^{-7} M.

pH-Triggered Release of CC from CC-Loaded Nanoassemblies. The release of CC was investigated at 25 °C under the following conditions: pH 7.4 (control), pH 7.0, pH 6.0, and pH 5.0. First, CC-loaded ATH1 nanoassemblies were prepared by the nanoprecipitation method, as described above. Next, the CC-loaded nanoassembly solutions at pH 7.4 were adjusted to pH 7.0, 6.0, and 5.0 using a buffer solution at pH 1.0. The release of CC was tracked by monitoring the time evolution of the fluorescence emission intensity of CC-loaded nanoassemblies (CC, $\lambda_{\rm ex}$ = 430 nm, $\lambda_{\rm em}$ = 516 nm).

Reductive-Triggered Release of CC from CC-Loaded Nanoassemblies. The release of CC was investigated at 25 °C under different concentrations of DTT: 5.0, 10.0, and 15.0 mM. First, CC-loaded ATH1 nanoassemblies were prepared by a nanoprecipitation method, as described above. Next, micellar solutions containing 5.0, 10.0, and 15.0 mM DTT were obtained by the addition of the required amount of aqueous DTT solution (0.1 M) to reach the targeted concentration. The release of CC was tracked by monitoring the time evolution of the fluorescence emission intensity of CC-loaded nanoassemblies (CC, $\lambda_{\rm ex}$ = 430 nm, $\lambda_{\rm em}$ = 516 nm).

Dual-Stimuli-Triggered Release of CC from CC-Loaded Nanoassemblies. The release of CC was investigated by applying sequential and additive reductive and acid treatments. First, the colloidal dispersion of CC-loaded ATH1 nanoassemblies (pH 7.4) was adjusted to 15 mM DTT, as described above. After 3 h, the pH of the solution was adjusted to pH 5.0 to subject the release process to cotriggered conditions. The release of CC was tracked by monitoring the time evolution of the fluorescence emission intensity of CC-loaded nanoassemblies (CC, $\lambda_{ex} = 430$ nm, $\lambda_{em} = 516$ nm).

Cell Viability Assays. Cellular cytotoxicity was assessed in two human cancer cell lines: HT-29 and HeLa cells. The cell viability experiments were carried out in three conditions: cells in the presence of the blank ATH1 polymer as a control, CC-loaded ATH1 nanoassemblies, and free CC. The cells were plated in 96-well plates (8000 cells/100 μ L/well in HeLa cells; 9000 cells/100 μ L/well in HT-29 cells) with supplemented DMEM without phenol red. After 24 h, several serial dilutions of the polymer and CC were added to the cells. The maximum tested concentration of ATH1 was 300 μ g/mL, and in the case of CC, it was 16.8 μ g/mL. The cells were incubated in the presence of the compounds during 48 h, and after this period, the cytotoxicity was checked by adding the CellTiter reagent. The CellTiter 96 AQueous One Solution Cell Proliferation Assay Kit (Promega, Madrid, Spain) provides a convenient and sensitive procedure for determining the number of viable cells in cytotoxicity assays. The CellTiter reagent (20 μ L, 1/4 dilution in DMEM without phenol red) was added into each well of the 96-well assay plate containing the samples. The plate was incubated at 37 °C for 2 h under a humidified 5% CO₂ atmosphere, and later, the absorbance was recorded using the Synergy HT (BioTek) plate reader and the Gen5 1.10 software at 490 nm (reference wavelength: 800 nm). Each experiment was performed in triplicate and repeated at least two times.

Cell Uptake Studies. The cellular uptake of CC was studied toward HeLa and HT-29 cells using fluorescence microscopy. Cells were seeded in a 24-well culture plate at a density of 80,000 cells/ $500 \, \mu L$ /well in the case of HeLa cells and 90,000 cells/ $500 \, \mu L$ /well in the case of HT-29 cells. After 24 h of culture, the cells were treated with a polymer, CC-loaded nanoassemblies, or free CC for 24 h. The maximum concentrations of the polymer were 120 and $6.72 \, \mu g/mL$ in the case of curcumin. During this incubation, the cells were monitored continuously under a confocal microscope. Images were taken every 30 min during 24 h by employing both bright field microscopy and a GFP fluorescence filter. Each experiment was repeated at least three times.

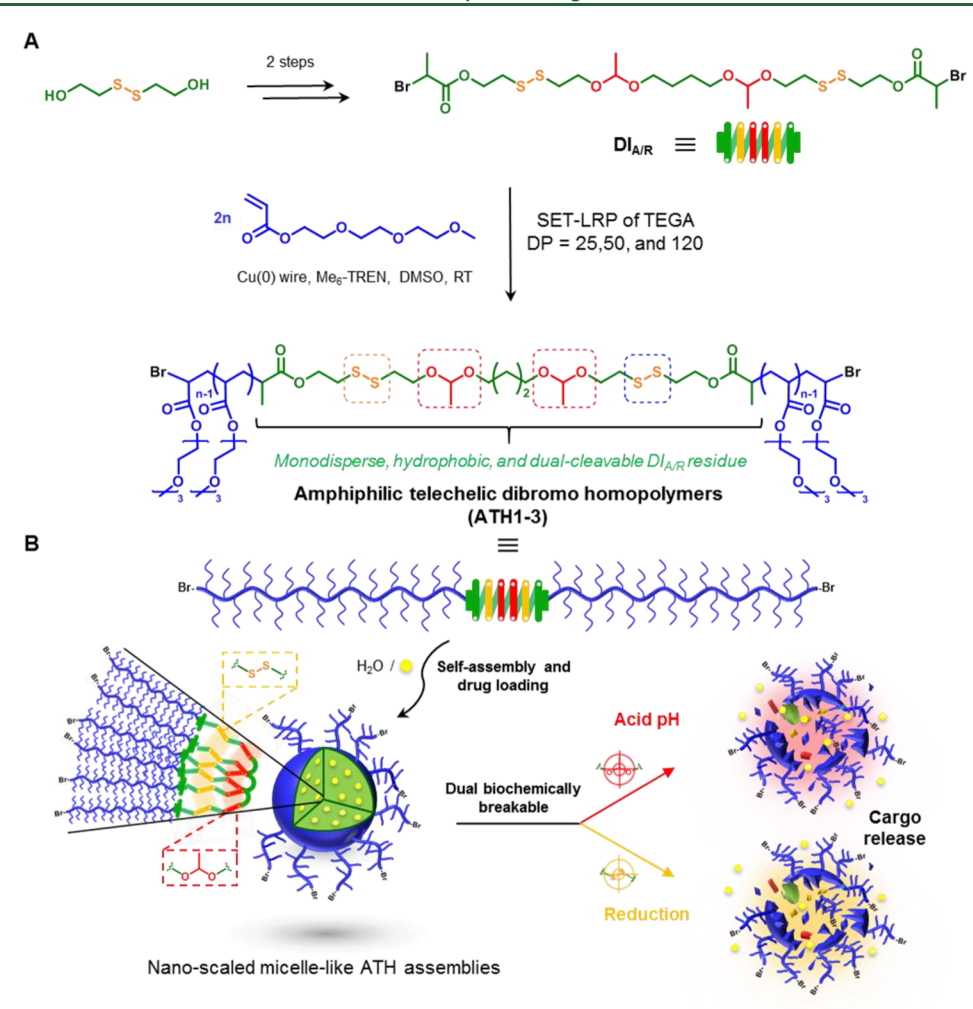


Figure 1. Schematic illustrating the design and construction of dual biochemically breakable micellelike nanocarriers via the self-assembly of programmed fully hydrophilic TEGA homopolymers. (A) Synthesis of $DI_{A/R}$ as a hydrophobic initiator containing double acetal and disulfide linkages and subsequent SET-LRP synthesis of ATH1-3 homopolymers from the TEGA monomer using copper wire and Me_6 -TREN in DMSO at 25 °C. (B) Aqueous self-assembly of ATH1-3 into pH- and reduction dual-responsive micellelike nanocarriers for hydrophobic drugs. Color code: blue, hydrophilic and water-soluble linkages; green, hydrophobic and water-insoluble linkages; red, acidic pH-sensitive acetal linkages; and orange, reduction-sensitive disulfide linkages. Detailed synthesis and characterization of $DI_{A/R}$ are available in an earlier work (see Figures S1-S3).

Table 1. Characterization of the TEGA Homopolymers and Their Self-Assembly Parameters in Aqueous Media

ATH^a	DP^{b}	Conv. ^c (%)	$\frac{M(\mathrm{th})^d}{(\mathrm{Da})}$	$M_{\rm n}^{\ e}$ (Da)	$M_{ m w}/M_{ m n}^{e}$	$M_{\rm n}^{f}$ (Da)	DIR ^g (wt %)	D_z^h (nm)	PDI ^h	D_{z}^{i} (nm)	PDI^i	$CAC^{j}(mg \cdot L^{-1})$
1	25	91	5400	6400	1.23	5700	8.4	5 ± 1	0.29 ± 0.06	79 ± 4	0.13 ± 0.02	1.7
2	50	95	10,230	11,010	1.24	10,800	5.0	6 ± 2	0.29 ± 0.08	127 ± 2	0.15 ± 0.03	2.1
3	120	87	26,190	30,500	1.25	24,700	1.8	4 ± 2	0.34 ± 0.03	175 ± 5	0.21 ± 0.03	4.3

^aPolymerization conditions: TEGA = 0.5 mL, DMSO = 0.25 mL, and $[DI_{A/R}]_0/[Me_6$ -TREN] $_0$ = 1/0.2 using 4.5 cm of hydrazine-activated copper wire, 20 gauge, at 25 °C for 2 h. ^bCalculated from the $[TEGA]_0/[DI_{A/R}]_0$ ratio. ^cDetermined by ¹H NMR. ^dM(th) = 218.2 × $[TEGA]_0/[DI_{A/R}]_0$ × conv. + 720.6. ^eDetermined by GPC in THF using PMMA standards. ^fDetermined by ¹H NMR. ^gWeight fraction of the hydrophobic initiator residue in the whole hydrophilic ATH. ^hDLS results of solutions in CHCl₃ at 20 mg·mL⁻¹ (25 °C) presented as the mean ± standard deviation of three replicates. ^fDLS results of colloidal solutions in water at 1 mg·mL⁻¹ (25 °C) presented as the mean ± standard deviation of three replicates. ^fCritical aggregation concentration determined by fluorescence spectroscopy using Nile Red as a probe.

■ RESULTS AND DISCUSSION

Preparation and Characterization of ATHs. The high degree of structural control and chain-end fidelity enabled by SET-LRP allows the preparation of well-defined telechelic dibromopolymers featuring single⁴⁷ and multiple⁴² cleavage units at the chain center by using cleavable DIs.

Herein, amphiphilic telechelic homopolymers [poly(TEGA)-s, ATH1-3, see Figure 1A], consisting of two fully hydrophilic and water-soluble blocks connected by a monodisperse,

hydrophobic, and dual cleavable initiator residue, were synthesized using the sequence-encoded α -haloester-type initiator $\mathrm{DI}_{\mathrm{A/R}}$ (Figure 1A). Surface-activated copper wire was used as a unique metal source, and tris[2-(dimethylamino)-ethyl]amine (Me₆-TREN) was used as a disproportionation-favoring ligand to conduct SET-LRP in DMSO. ⁴⁸ The ratio of the TEGA monomer to the initiator was varied from 25 to 120 to yield symmetric homopolymers with increasing chain lengths while retaining a low weight percentage of the hydrophobic

initiator residue (<8.5 wt %). The polymerization results are presented in Table 1.

SET-LRP reactions at 25 °C were fast, reaching up to $\approx 90\%$ conversion within 2 h. A representative kinetic study targeting a degree of polymerization (DP) of 50 (25 for each two initiating sites) revealed that the homopolymerization of TEGA occurred in a controlled manner, as all features of living polymerization kinetics were indeed displayed, e.g., linear semilogarithmic kinetic plot, with good agreement between the measured $M_{\rm n}^{\rm GPC}$ and the theoretical $M({\rm th})$ values that are retained up to high conversion (Figure 2A). After the synthesis, the three produced

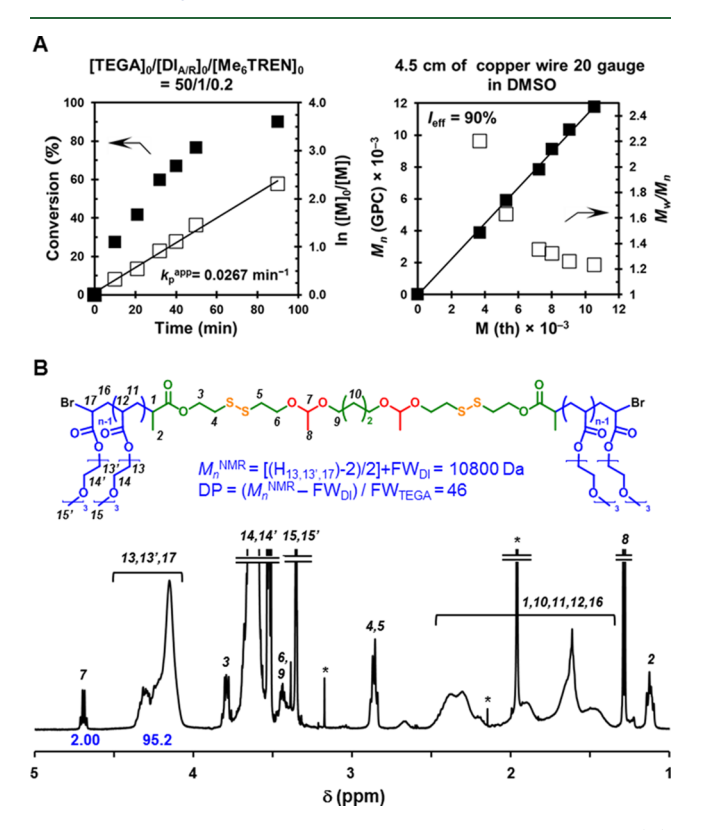


Figure 2. SET-LRP synthesis of ATHs from TEGA and $DI_{A/R}$. (A) Monomer conversion, kinetics plots, and evolution of experimental M_n (GPC) and M_w/M_n , based on the calibration by PMMA standards versus theoretical M(th) for the SET-LRP of TEGA initiated from $DI_{A/R}$ in DMSO. Reaction conditions: TEGA = 0.5 mL, DMSO = 0.25 mL, $[\text{TEGA}]_0/[DI_{A/R}]_0/[Me_6\text{-TREN}]_0 = 50/1/0.2$, and 4.5 cm of the hydrazine-activated copper wire, 20 gauge. (B) ^1H NMR spectrum of ATH2 in CDCl₃ (10 mg·mL $^{-1}$) at 25 °C. ^1H NMR resonances from residual nondeuterated solvents are indicated with asterisks.

ATHs (ATH1-3) were first purified before any further study by passing the diluted (THF) crude solution through a short basic alumina column to remove copper salt residues. Next, the eluate was exhaustively dialyzed against acetone (2.0 kDa MWCO) to remove residual monomer and furnish sticky clear solids once concentrated. GPC analysis revealed relatively narrow peaks ($M_{\rm w}/M_{\rm n}$ <1.25) and confirmed that the molecular weight of ATHs increased from ATH1 to ATH3 while agreeing well with the targeted values (Table 1). The structure of the synthesized ATHs was further characterized by $^1{\rm H}$ NMR spectroscopy, as depicted in Figure 2B and Figures S4 and S5.

The typical proton peaks of the both pendant and main chain-repeating unit structure, e.g., 4.0–4.5 ppm, and the initiator residue integrating acetal, e.g., 1.1 ppm, and disulfide, e.g., 2.8

ppm, junctions were clearly observed, proving the successful polymerization. Furthermore, molecular weight and DP values of target ATHs, determined by comparing the ¹H NMR peak at 4.7, i.e., attributed to the acetal methine protons at the initiator residue, with those between 4.0 and 4.5 ppm, i.e., attributed to the polymer end and side groups, proved to be consistent with theoretical and GPC values (Figure 2B and Table 1). Finally, the symmetric architecture of the synthesized homopolymers was confirmed by conducting site-selective middle-chain cleavage studies on the dissolved polymers under both acidic and reductive conditions (vide infra). Overall, these results demonstrated the successful synthesis of ATHs via SET-LRP.

Self-Assembly of ATHs in Aqueous Solutions. As detailed previously, hydrophilic homopolymers as well as random copolymers with either hydrophobic end(s)^{13–17} or middle groups^{39,40} can self-assemble in aqueous solution into regular nanoassemblies, including micelles, vesicles, and flower-like complex particles. In our case, the aggregation of folded ATH chains was expected to form in aqueous solutions micelle-like nanoassemblies, with the dual acidic pH and the reduction-activated initiator residue serving as the inner core and the hydrophilic poly(TEGA) arms as the outer corona (Figure 1B).

As a first step in characterizing the self-assembly behavior, CAC values were determined by a fluorescent probe molecule method using Nile Red.⁴⁹ As shown in Figure 3A, negligible fluorescence was detected at low polymer concentrations, although suddenly an abrupt change in the intensity was observed above a critical concentration, indicating the incorporation of the Nile Red molecules into the hydrophobic core of the formed micelle-like nanoassemblies. Hence, ATH1 has a low apparent CAC of about 1.7 mg· L^{-1} . Interestingly, CAC values determined graphically from the intersection of the two lines appeared to be higher for homopolymers with longer poly(TEGA) segments due to a higher hydrophilic character (see Table 1). However, when considering the increase in the molecular weight in ATH1-3, the CACs of the three homopolymers are relatively closer to each other. Next, the self-assembly of ATHs in aqueous solution was induced using a nanoprecipitation method, i.e., slow injection of water droplets into the polymer in THF solution (THF/water ratio = 1/7), to obtain thermodynamically stable self-assembled nanostructures. The samples were prepared at 1 mg·mL⁻¹, which was a higher concentration than the CAC. The hydrodynamic diameter (D_h) and the morphology of the resulting nanoassemblies were characterized by dynamic light scattering (DLS) and transmission electron microscopy (TEM). As shown in Figure S6, ATH1 self-assembled into well-dispersed nanoparticles with an average diameter well below 100 nm, i.e., $D_h = 79 \pm 0.4$ nm and polydispersity index (PDI) = 0.13 ± 0.02 . As expected, the selfassembly of ATH1 could also be accomplished by direct dispersion in water, although this less time-consuming preparation led to slightly larger and broader particles (Figure S7). The size and PDI of the nanoassemblies increased with the poly(TEGA) molecular weight because hydrophilic arms are extended in water (Figure 3B). Also TEM analyses demonstrated the formation of spherical nanoassemblies with a welldefined exterior boundary and a slightly darker core (Figure 3C). However, the size of these nanoparticles is not in agreement with the presence of simple unimolecular micelles, with homopolymer chains adopting a folded chain structure (Figure 1B). Further concentration-dependent measurements (0.1-20.0 mg·mL⁻¹) pointed toward a transition from watersoluble single random coil chains to small unimolecular micelles

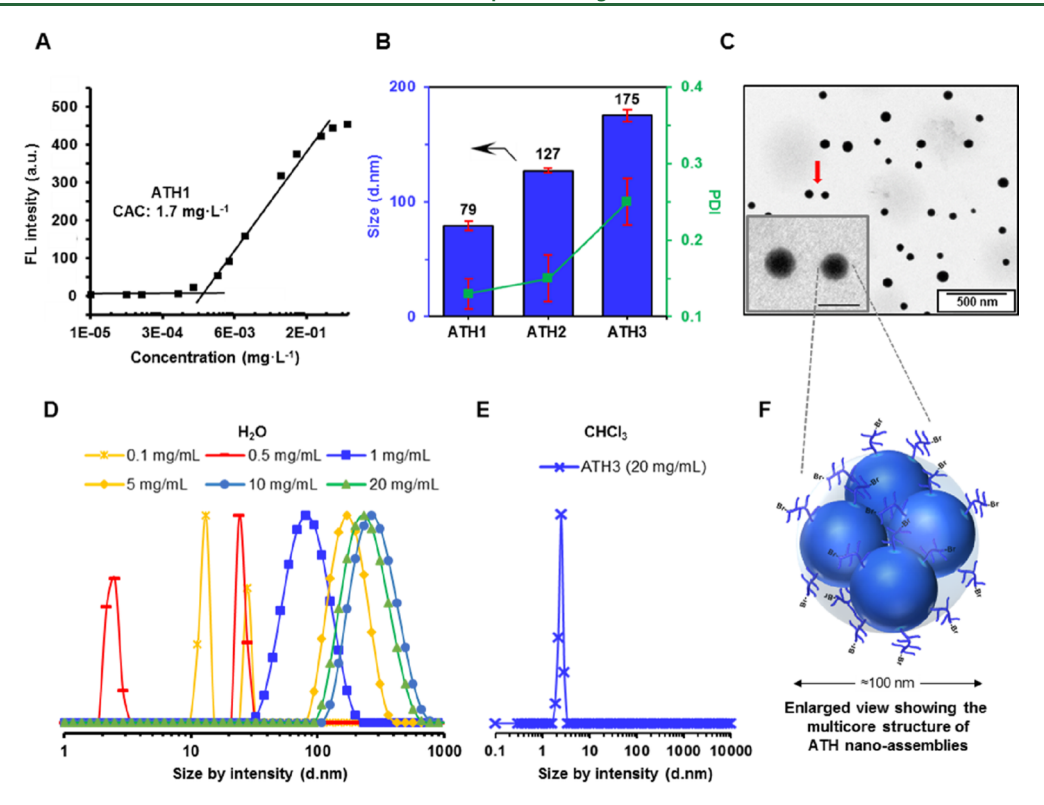


Figure 3. Self-assembly behavior of ATHs. (A) Plot of the fluorescence intensity from the NR emission at 625 nm ($\lambda_{\rm exc}$ = 550 nm) vs the logarithm of the ATH1 concentration. (B) DLS size and PDI for self-assembled ATHs in aqueous solution by the nanoprecipitation method (1 mg·mL⁻¹). (C) Nonstained TEM image of ATH1 nanoassemblies (1 mg·mL⁻¹). Scale bar is 100 nm. (D) DLS data for ATH1 nanoassemblies in the aqueous solution as a function of the polymer concentration (pH 7.4, 25 °C). (E) DLS data for ATH3 in CHCl₃ (1 mg·mL⁻¹). (F) Schematic illustration of the unimolecular multimicelle aggregates of ATH formed by the aggregation of small micelles (the size of the small micelles is magnified).

that are just intermediates because they further aggregate into unimolecular multimicelle aggregates with a multicore structure upon increasing the concentration (Figure 3D). 50-53 As a control, DLS analysis in a good organic solvent for both poly(TEGA) arms and the initiator residue revealed the presence of single random coil chains with D_h<5 nm rather than self-assembled nanostructures even at a high concentration (Figure 3E). Since the weight fraction of the hydrophobic initiator residue in the whole hydrophilic ATHs is tiny, while the amount of water is large, the high water polarity and the energy state of nanoparticles might be driving the assembly of single random coil chains into small micelles in the state of a high energy due to unfavorable amphiphilicity.⁵⁴ According to the fact that the larger particles are more energetically stable than the smaller ones, 55 these small micelles aggregate spontaneously until the size is large enough to make the formed nanoassemblies, i.e., unimolecular multimicelle aggregates, stable in the polar environment (Figure 3F). Intermicellar interactions through hydrophilic coronas must also be contributing to the overall self-aggregation process. 56-58 This contribution is also reasonable based on the above-mentioned observation that the size of the nanoassemblies increased with an increase in the molecular weight of the hydrophilic homopolymer (Figure 3B). ATHs with longer hydrophilic block lengths are more prone to form larger clusters, e.g., unimolecular multimicelle aggregates. Since the micellar self-assembly of this new class of amphiphilic homopolymers was demonstrated, we envisioned great potential scope in drug encapsulation and delivery because degradable acetal and disulfide functionalities were expected to act as a "keystone" for the particles under relevant biochemical conditions.

pH- and Reduction-Triggered Breakdown of ATH Nanoassemblies. It is known that the acetal and disulfide linkages can be selectively and even orthogonally disconnected upon exposure to biologically relevant input signals, i.e., acidic pH and reductive conditions, respectively. 33,44,59 Accordingly, we expected that the decrease to half value in the molecular weight of ATHs upon site-selective cleavage at their core unit should dramatically impact their solubility behavior in aqueous solution. 39,40 To verify dual-responsive properties, we monitored the stability of the ATH1 nanoassemblies under different biomimetic conditions by DLS (Figure 4A–C). Upon exposure to pH 7.4 buffer conditions similar to normal physiological environments, the nanoparticles showed a remarkable dimensional stability and maintain a stable size of around 80 nm for at least 12 h (Figure 4A). Stability in terms of the nanoparticle morphology and size was also demonstrated by TEM (Figure S8). However, declining the pH value to 5.0 evidently activated the breakdown of the nanoassemblies (Figure 4B). DLS analysis revealed that the complete dissolution of the particles occurred in a time scale of 12 h, which may be advantageous for designing sustained drug delivery at specific acidic sites, e.g., tumor tissues. 43 Interestingly, the breakdown of the self-assembled particles occurred through an increasing-decreasing profile (Figure S9), suggesting that it follows a swelling-to-crack mechanism driven by the acid hydrolysis of acetal linkages (Figure 4D). TEM was employed to visualize the remarkable expansion of the nanoassemblies (Figure S10). The cleavage of the acetal linkages was further demonstrated by GPC because when the THF-dissolved symmetric polymer was treated with acid, a decrease in the polymer size by a factor of 2 was observed, with the retention of the monomodality and narrow molecular

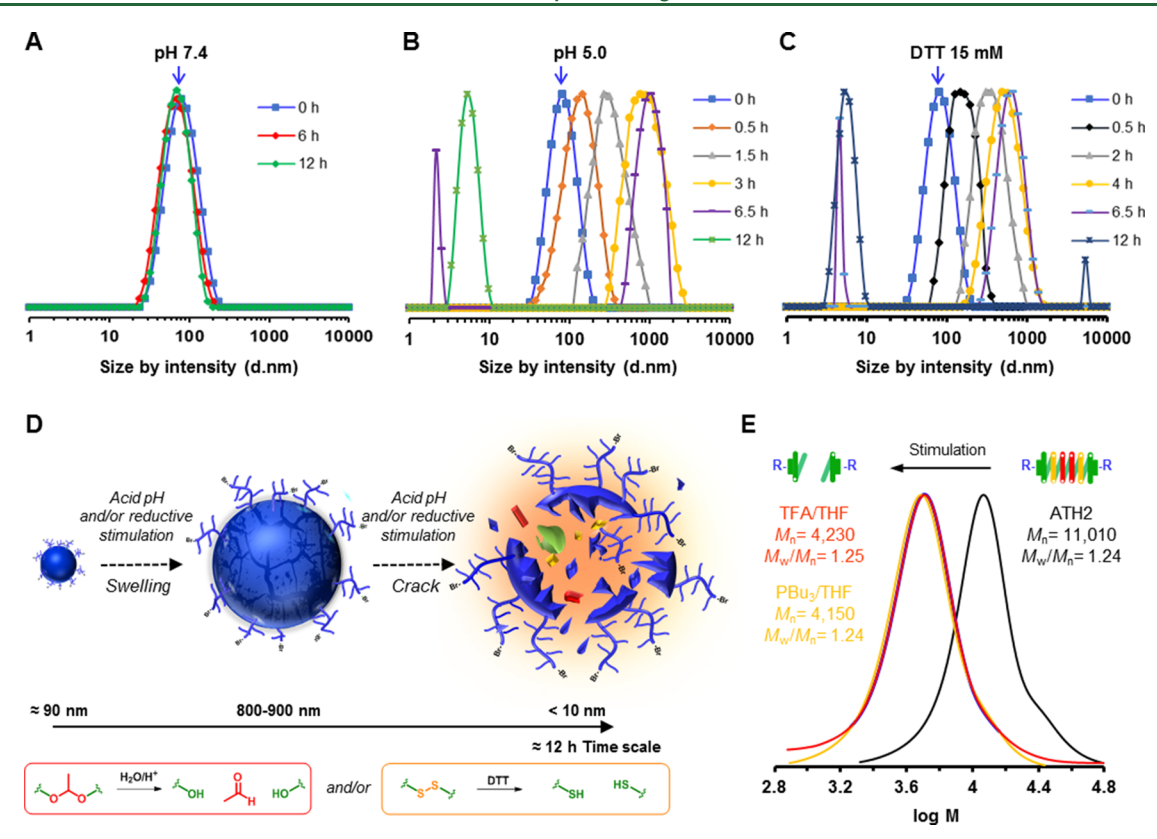


Figure 4. pH- and reduction-triggered breakdown of ATH nanoassemblies. (A) Size change through time of ATH1 nanoassemblies in response to (A) pH 7.4, (B) acid pH treatment (pH 5.0), and (C) reductive treatment (15 mM DTT). DLS traces at t_0 are indicated by blue arrows. (D) Schematic of the pH/reduction dual-triggered "swell-crack" breakdown of ATH nanoassemblies via the cleavage of acetal and/or disulfide linkages. (E) GPC traces for ATH2 dissolved in THF before (black line) and after either acidic pH (0.1 M trifluoroacetic acid, red line) or reductive (100 equiv PBu₃, orange line) treatments. Both treatments were conducted for 60 min to promote the middle-chain cleavage of the telechelic architecture. Note that the polymer chains in the schematic illustrations shown in (E) are indicated by (-R) for simplicity.

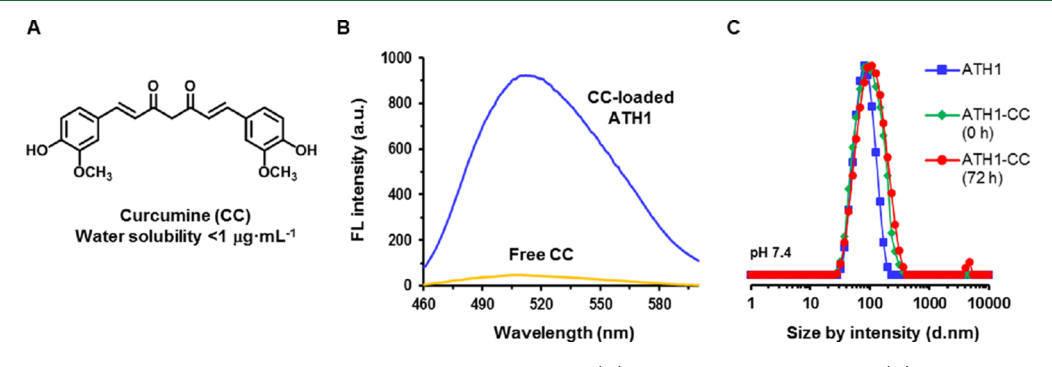


Figure 5. Encapsulation of a hydrophobic CC drug into ATH1 nanoassemblies. (A) Chemical structure of CC. (B) Fluorescence spectrum of CC-loaded ATH1 nanoassemblies and free CC in aqueous solutions at equivalent concentrations of drug. (C) DLS measurements to study the stability of CC-loaded ATH1 nanoassemblies (1 mg polymer·mL⁻¹) at pH 7.4. Data for nonloaded particles are included for comparison purposes.

weight distribution, indicating the site-selective disconnection of the two-arm homopolymer into two equal-sized fragments (Figure 4E).⁴²

This is an additional proof of the symmetric telechelic structure of the synthesized polymers. When a colloidal dispersion comprising ATH1 nanoassemblies was treated with DTT (15 mM), the size of the nanoparticles also markedly enlarged prior to their breakdown into soluble unimers of <10 nm, demonstrating the cleavage of disulfide bonds and the dissociation of the aggregation under reductive conditions (Figure 4C and Figure S9). The size expansion of nanoassemblies occurring upon reductive stimulation was also confirmed by TEM (Figure S11). Reductive splitting of the

dissolved telechelic polymer was further demonstrated by GPC (Figure 4E). Overall, DLS and GPC measurements clearly demonstrate the favorable dual pH and reduction-responsive self-assembly behavior of the conceived simple ATH nanoassemblies, making these materials appealing for the design and preparation of antitumor drug carriers for cancer therapy owing to the fact that tumor cells and tissues show low pH and a high reducing environment. ^{35,45}

Drug Release Profiles from ATH Nanoassemblies. The potential of ATH1 nanoassemblies to load and deliver hydrophobic chemotherapeutic agents was investigated using CC as a model hydrophobic drug (Figure 5A). This polyphenolic compound, chemically identified as (1*E*,6*E*)-1,7-

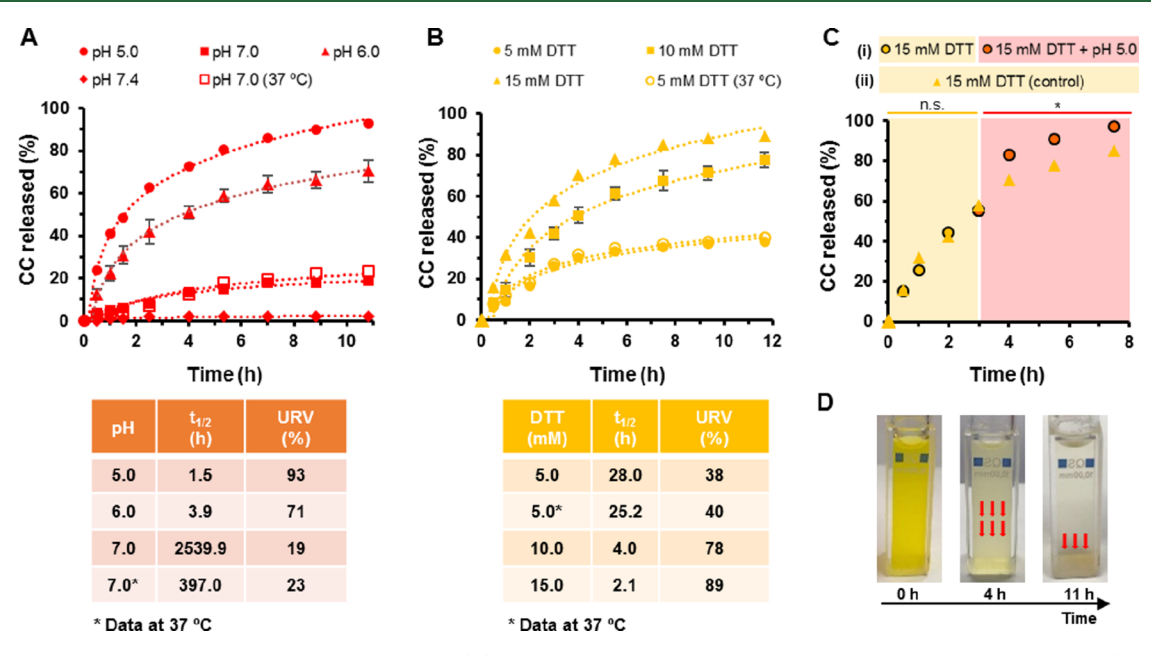


Figure 6. In vitro release of CC from ATH1 nanoassemblies. (A) CC release profile from ATH1 nanoassemblies in aqueous solution (1 mg polymer-mL⁻¹) in response to various pH values. (B) CC release profile from ATH1 nanoassemblies in aqueous solution (1 mg polymer-mL⁻¹) in response to various DTT concentrations. The dotted lines in A and B are the logarithmic fitting curves of the data points, $t_{1/2}$ is the half-release time of CC, and URV is the ultimate release value at the end of each drug release experiment. All the experiments were conducted at 25 °C unless otherwise noted. (C) CC release profile from ATH1 nanoassemblies in aqueous solution (1 mg polymer-mL⁻¹) in response to (i) reductive-acid sequential additive (15 mM DTT for 3 h and 15 mM DTT/pH 5.0 for 5 h) and (ii) control 15 mM DTT (8 h) treatments. Both treatments are not statistically significant from each other during the first 3 h (n.s., two-way ANOVA without replication) but are significantly different once the pH is reduced to 5.0 in treatment (i) (*p-value = 0.002). (D) Representative digital images taken at different time periods during the release of CC from ATH1 nanoassemblies.

bis (4-hydroxy-3-methoxyphenyl)-1,6-heptadiene-3,5-dione, is a popular pleiotropic active agent due to its abundant therapeutic properties,⁶⁰ among which is the ability to induce selective apoptosis to various tumor cells.^{61,62}

The extremely low aqueous solubility of this drug (<1 μ g· mL⁻¹) as well as instability at physiological pH has stimulated the intensive search of nanosized vehicles for efficient intracellular CC delivery. 30,62-64 Herein, CC-loaded nanoassemblies were prepared by co-nanoprecipitation starting from a solution containing both the amphiphilic homopolymer (ATH1) and the hydrophobic drug (CC) (see the Experimental Section for details). We first confirmed the noncovalent encapsulation of CC via fluorescence spectroscopy analysis of the obtained bright yellow aqueous colloidal solution. As can be seen in Figure 5B, the poorly water-soluble CC only showed its characteristic intense emission peak at 516 nm when loaded into the hydrophobic cores of the nanoparticles. Note that the CC loading content and encapsulation efficiency values achieved with our designed amphiphilic homopolymer, i.e., 8.1 and 81.0%, respectively, are highly competitive compared to other CC carriers based on block copolymers. 30,64 After drug encapsulation, DLS analysis revealed a slight particle expansion (from 79 to 95 nm), which is consistent with the entrapment of the drug into the core reservoir of the nanoassemblies (compare squares and diamonds in Figure 5C). The prepared CC-loaded nanoparticles demonstrated to be stable for at least 72 h (circles in Figure 5C).

Next, we turned to evaluate the in vitro acid-triggered release of CC from the loaded nanoassemblies by tracing its fluorescent intensity upon exposure to the following conditions: pH ranging from 5.0 to 7.4 or 5.0 to 15.0 mM DTT. Note that for efficient antitumor drug delivery systems, nanocarriers are expected to be stable during circulation in the blood while also releasing the

encapsulated drugs rapidly after entering the tumor cells. Preliminary control experiments demonstrated negligible CC release under conditions mimicking the normal physiological environment (PBS, pH 7.4) (diamonds in Figure 6A). However, as shown in Figure S12, a progressive decrease in the fluorescence intensity occurred throughout the incubation at pH 5.0. Under these conditions, the ultimate release value (URV) after 11 h was about 93% (circles in Figure 5A).

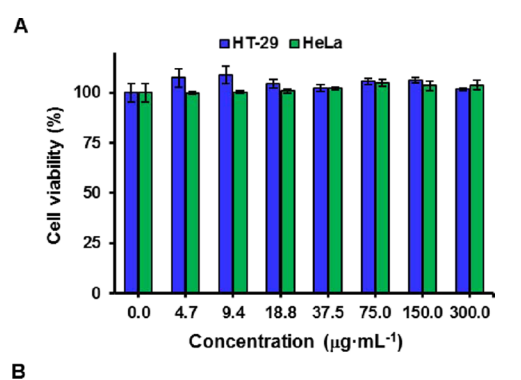
As expected, the release kinetics decreased with increasing pH of the soaking buffer. 59 For instance, the release rate decreased by a factor of around 2 times when the pH was increased from 5.0 to 6.0. However, it is noteworthy to mention that the system provided short half-release times $(t_{1/2})$ under conditions mimicking acidic intracellular environments inside the endosome and the lysosome (pH 4.5-6.5). Conversely, the CC release tended to equilibrium at about 20% at a pH closer (pH 7.0) to that which is characteristic of extracellular healthy environments (pH 7.4). Note that data from an in vitro CC release experiment at 37 °C were comparable to that obtained at 25 °C (compare solid and empty squares in Figure 6A). To validate reduction-triggered drug release, in vitro drug release behaviors were also investigated in PBS (pH 7.4) in the presence of various concentrations of DTT. As shown in Figure 6B, the CC release rate in response to conditions mimicking intracellular tumor reductive microenvironments (10 mM DTT) was almost similar to that at pH 6.0 (compare triangles with squares in Figure 6A,B, respectively). Incubation with 15 mM DTT further accelerated the drug release. Under these conditions, almost 90% of the loaded CC was released from the nanoassemblies ($t_{1/2} = 2.1$ h). However, a very slow release was observed with 5 mM DTT just reaching about 40% in 12 h both at room temperature (25 °C) and at body temperature (37 °C) (filled and empty circles in Figure 6B). Furthermore, fine-

tuned release modes were also accessible under cotriggered conditions. As can be seen in Figure 6C, improved release behavior was observed under the effect of dual factors when applying simultaneously reductive and acid treatments (15 mM DTT and pH 5.0) after a short period of exclusive reductive stimulation. The same protocol can be applied starting first with acidic conditions (Figure S13). Throughout all these in vitro drug release studies, the CC release process could also be visually monitored because the experiment solution progressively turned from bright yellow to colorless, while poorly watersoluble CC precipitated at the bottom of the cuvette (Figure 6D). This series of experiments suggest that ATH1-CC nanoassemblies may rapidly release cargo in response to acid/reductive microenvironments proposed during endocytosis into cancer cells. 65

In Vitro Cytotoxicity and Cellular Uptake. Encouraged by the above reported findings, we were interested in testing the potential of using our simple CC-loaded nanoparticles in living cells. Two cell lines, HeLa, a human cervix epithelioid carcinoma cell line, and HT-29, a human colon adenocarcinoma cell line, were used as models. Prior to assessing the biological activity of the encapsulated CC, the effect of empty ATH1 nanoassemblies in cell viability was determined in both cell lines using the CellTiter 96 AQueous One Solution Cell Proliferation Assay Kit (Promega) as the reactive. The homopolymer in study did not exhibit relevant toxic effects (>95% cell viability) up to a concentration of 300.0 μ g·mL⁻¹ (Figure 7A), a compound concentration that is considered enough to meet most drug delivery requirements.

Confocal microscopy images obtained during the cell culture were analyzed, and the effect of assemblies on cell morphology was determined (Figure 7B and Figure S12). In the presence of the polymer (120 μ g·mL⁻¹), both cell lines showed normal proliferation with no changes in cell morphology when compared to nontreated cells (used as controls). For example, both nontreated and treated HeLa cells were adherent and exhibited their typical smooth surface and elongated structure (Figure 7B). No noticeable morphological changes were observed in the HT-29 cell line (Figure S14).

Next, the effect of treating HT-29 and HeLa cells with CCloaded ATH1 nanoassemblies in comparison with free CC was investigated. As shown in Figure 8A,B, the half-maximal inhibitory concentration (IC50) of CC-ATH1 treatment was lower in comparison with free CC, which could be explained due to the enhanced aqueous solubility of CC in the nanoparticles in combination with accelerated acid-/reductive-triggered release of CC in the tumor environment or after endocytosis in the endosomes or lysosomes.⁶⁵ It is important to note that CC did not promote cytotoxicity in the HT-29 cell line at a concentration below 16.8 μg·mL⁻¹ (cell viability over 90%), but the IC50 of CC-loaded nanoassemblies was about 8.3 μ g· mL⁻¹ (Figure 8A). On the other hand, the CC-loaded ATH1 possessed over 2.7-fold lower IC50 value than free CC also for the HeLa cell line (Figure 8B). These results demonstrate a greater effect in reducing the initial cell viability percentage when the cells are treated with the drug-loaded nanoformulation over free CC. As in the case of the empty assemblies, confocal microscopy was used to observe the morphological changes in the cells at early stages of the drug release process to provide qualitative information about the effect in the cells. The green intrinsic fluorescence of CC seems to be detected after 1 h inside HT-29 cells after exposing to either CC-loaded nanoassemblies



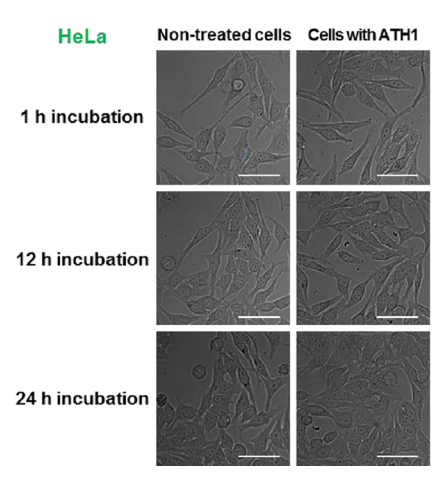


Figure 7. Cytotoxicity of empty ATH1 nanoassemblies against HT-29 and HeLa cell lines. (A) Cell viability values for HT-29 and HeLa cells determined by CellTiter 96 assay after 48 h of incubation with various concentrations of empty ATH1 nanoassemblies. All the data are presented as the average \pm standard deviation. (B) Confocal microscopy images of HeLa cell cultures nontreated and treated with ATH1 nanoassemblies. Images taken at different time periods (1, 12, and 24 h) at [ATH1]₀ = 120 μg·mL⁻¹. Scale bars represent 100 μm.

or free CC, suggesting that both systems undergo intracellular trafficking (Figure 8C).⁶⁶

HT-29 cells incubated with free drug retained the morphology of nontreated control cells, and they only started to show the overall shrinkage in their volume after 6 h (compare enlarged views 2, 5, and 8 with 1, 4, and 7). The white arrow in the enlarged view 8 indicates early cell shrinkage. However, what is more interesting is that they conversely showed more premature suffering when treated with CC-loaded nanoparticles (see enlarged views 3, 6, and 9). Early apoptotic bodies indicated by yellow arrows in the enlarged view 3 were already observed after 1 h. Moreover, intense fragmentation indicated by red arrows was observed at longer exposure times. Fluorescence microscopy results for HeLa cells also revealed that the use of CC-loaded ATH1 nanoparticles induced greater morphological disruption than free CC (Figure S15). These observations are consistent with previous observations with other CC-loaded nanoparticles and cell lines. 30,64 Overall, it has been demonstrated that our design based on programmed associative homopolymers could be considered a particularly interesting simplified platform for cancer chemotherapy.

CONCLUSIONS

Fully hydrophilic telechelic dibromopolymers with hydrophobic initiator residues precisely located at the center of the polymer

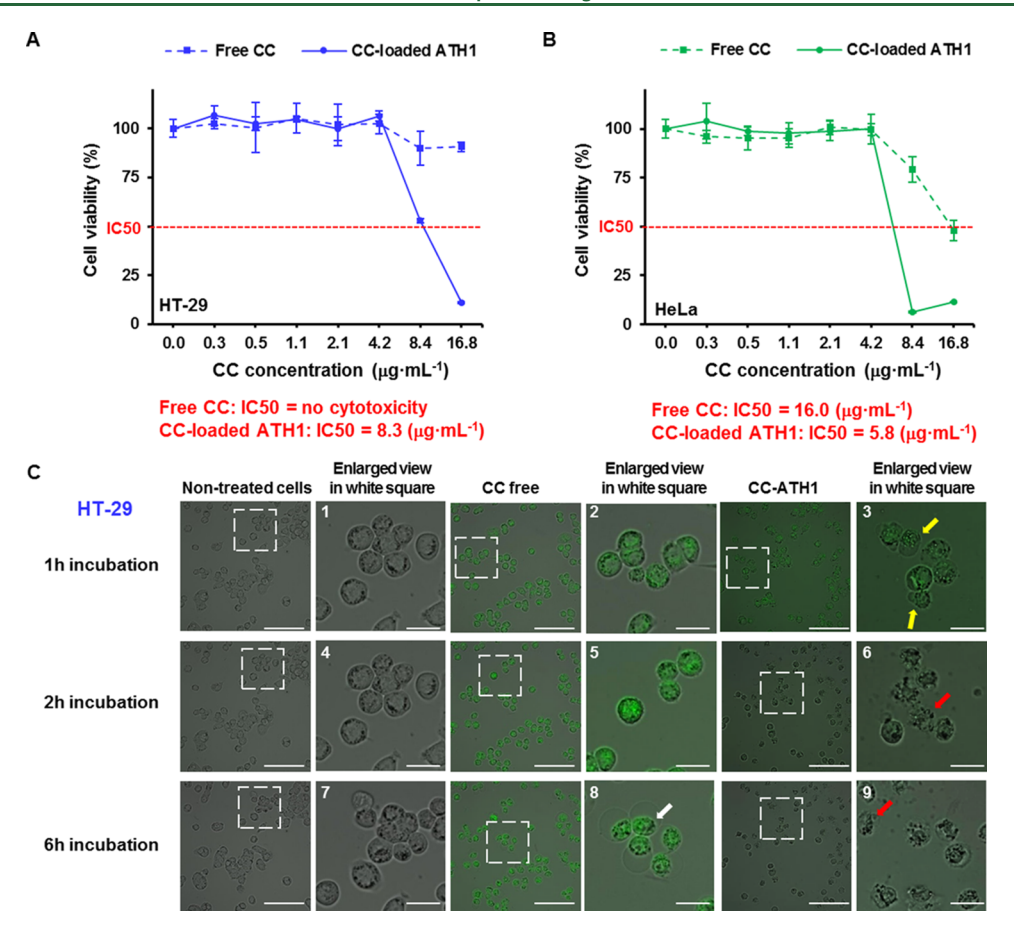


Figure 8. Cytotoxicity of CC-loaded ATH1 nanoassemblies against HT-29 and HeLa cells. Cell viability of HT-29 (A) and HeLa (B) cells after incubation with free CC and CC-loaded ATH1 nanoassemblies for 24 h at various CC concentrations. (C) Confocal images of HT-29 cells after incubation with free CC and CC-loaded ATH1 nanoassemblies for 1, 2, and 6 h ($[CC]_0 = 6.7 \,\mu\text{g·mL}^{-1}$). Images of nontreated cells are also shown for comparison purposes. The white arrow in the enlarged view 8 indicates cell shrinkage, yellow arrows in 3 indicate early apoptotic cells, and red arrows in 6 and 9 indicate nucleus fragmentation. Scale bars represent 100 μ m (25 μ m for the magnified sections).

chain can directly self-assemble in water to form micellelike nanoaggregates due to their amphiphilic nature. 39,40 Herein, SET-LRP served to grow biocompatible poly(TEGA)s chains from a designed α -haloester type sequence-encoded DI containing both acetal and disulfide bonds. With the initiator residue forming the core of these simple nanoscaled assemblies, the combination of CAC, DLS, GPC, TEM, and fluorescence spectroscopy measurements in simulated biochemical environments was used to demonstrate their breakdown along with the ongoing precise middle-chain cleavage. Accordingly, the in vitro drug release of CC was stimulated in both acidic pH and reductive conditions as well as cotriggered environments. Afterward, even though the homopolymers showed no cytotoxicity, the corresponding CC-loaded nanoparticles displayed more efficient growth inhibition of HT-29 and HeLa cells than free CC. The potential rich chemistry of the cleavable groups in difunctional and multifunctional initiators for SET-LRP offers a useful Lego-type platform for the fabrication of simple and smart drug-delivery vehicles by exploring the use of alternative commercial and designed hydrophilic monomers^{67,68} as well as exploiting the appealing high chain end fidelity of SET-LRP polymers. 69-71

ASSOCIATED CONTENT

Supporting Information

The Supporting Information is available free of charge at https://pubs.acs.org/doi/10.1021/acs.biomac.0c01113.

Materials and instrumentation; synthetic route for $\mathrm{DI}_{A/R}$ experimental procedures; additional DLS curves and TEM images for ATH nanoassemblies; evolution of DLS size as a function of time during the breakdown of nanoparticles; representative fluorescence spectra recorded during CC-release experiments; complementary confocal microscopy images; and cytotoxicity studies (PDF)

AUTHOR INFORMATION

Corresponding Authors

Gerard Lligadas — Laboratory of Sustainable Polymers,
Department of Analytical Chemistry and Organic Chemistry,
University Rovira i Virgili, Tarragona 43007, Spain; Roy &
Diana Vagelos Laboratories, Department of Chemistry,
University of Pennsylvania, Philadelphia, Pennsylvania 191046323, United States; orcid.org/0000-0002-8519-1840;
Email: gerard.lligadas@urv.cat

Adrian Moreno — Laboratory of Sustainable Polymers, Department of Analytical Chemistry and Organic Chemistry, University Rovira i Virgili, Tarragona 43007, Spain; Email: adrian.morenog@urv.cat

Authors

- Ana Jiménez-Alesanco Institute of Biocomputation and Physics of Complex Systems (BIFI), Joint Units IQFR-CSIC-BIFI, and GBsC-CSIC-BIFI, Universidad de Zaragoza, Zaragoza 50018, Spain
- Juan C. Ronda Laboratory of Sustainable Polymers, Department of Analytical Chemistry and Organic Chemistry, University Rovira i Virgili, Tarragona 43007, Spain
- Virginia Cádiz Laboratory of Sustainable Polymers, Department of Analytical Chemistry and Organic Chemistry, University Rovira i Virgili, Tarragona 43007, Spain
- Marina Galià Laboratory of Sustainable Polymers, Department of Analytical Chemistry and Organic Chemistry, University Rovira i Virgili, Tarragona 43007, Spain; orcid.org/0000-0002-4359-4510
- Virgil Percec Roy & Diana Vagelos Laboratories, Department of Chemistry, University of Pennsylvania, Philadelphia, Pennsylvania 19104-6323, United States; ⊚ orcid.org/0000-0001-5926-0489
- Olga Abian Institute of Biocomputation and Physics of Complex Systems (BIFI), Joint Units IQFR-CSIC-BIFI, and GBsC-CSIC-BIFI and Departamento de Bioquimica y Biologia Molecular y Celular, Universidad de Zaragoza, Zaragoza 50018, Spain; Instituto Aragonés de Ciencias de la Salud (IACS), Zaragoza 50018, Spain; Instituto de Investigación Sanitaria de Aragón (IIS Aragon), Zaragoza 50009, Spain; Centro de Investigación Biomédica en Red en el Área Temática de Enfermedades Hepáticas Digestivas (CIBERehd), Madrid 28029, Spain

Complete contact information is available at: https://pubs.acs.org/10.1021/acs.biomac.0c01113

Author Contributions

The manuscript was written through contributions of all authors. All authors have given approval to the final version of the manuscript.

Notes

The authors declare no competing financial interest.

ACKNOWLEDGMENTS

Spanish Ministerio de Ciencia, Innovación y Universidades through project MAT2017-82669-R (to G.L. and J.C.R) and FPI grant BES-2015-072662 (to A.M.) and the Serra Hunter Programme of the Government of Catalonia (to G.L.) are acknowledged for supporting and funding this work. Miguel Servet Program from Instituto de Salud Carlos III (CPII13/ 00017 to O.A.); Fondo de Investigaciones Sanitarias from Instituto de Salud Carlos III; European Union (ERDF/ESF, 'Investing in your future') (PI18/00343 to O.A.); Diputación General de Aragón (Predoctoral Research Contract 2019 to A.J-A., 'Digestive Pathology Group' B25 20R to O.A.); and Centro de Investigación Biomédica en Red en Enfermedades Hepáticas y Digestivas (CIBERehd). V.P. gratefully acknowledges the support from the National Science Foundation Grants DMR-1066116 and DMR-1807127 and the P. Roy Vagelos Chair at the University of Pennsylvania.

REFERENCES

(1) Men, Y.; Li, W.; Janssen, G. J.; Rikken, R. S. M.; Wilson, D. A. Stomatocyte in Stomatocyte: A New Shape of Polymersome Induced via Chemical-Addition Methodology. *Nano Lett.* **2018**, *18*, 2081–2085. (2) van Hest, J. C. M.; Delnoye, D. A. P.; Baars, M. W. P. L.; van Genderen, M. H. P.; Meijer, E. W. Polystyrene-Dendrimer Amphiphilic

- Block Copolymers with a Generation-Dependent Aggregation. *Science* **1995**, 268, 1592–1595.
- (3) Nyström, A. M.; Wooley, K. L. The Importance of Chemistry in Creating Well-Defined Nanoscopic Embedded Therapeutics: Devices Capable of the Dual Functions of Imaging and Therapy. *Acc. Chem. Res.* **2011**, *44*, 969–978.
- (4) Ueda, M.; Hashidzume, A.; Sato, T. Unicore-Multicore Transition of the Micelle Formed by an Amphiphilic Alternating Copolymer in Aqueous Media by Changing Molecular Weight. *Macromolecules* **2011**, *44*, 2970–2977.
- (5) Rodríguez-Hernández, J.; Checot, F.; Gnanou, Y.; Lecommandoux, S. Toward 'Smart' Nano-Objects by Self-Assembly of Block Copolymers in Solution. *Prog. Polym. Sci.* **2005**, *30*, 691–724.
- (6) Vasilevskaya, V. V.; Govorun, E. N. Hollow and Vesicle Particles from Macromolecules with Amphiphilic Monomer Units. *Polym. Rev.* **2019**, *59*, 625–650.
- (7) Zhang, J.; Liu, K.; Müllen, K.; Yin, M. Self-Assemblies of Amphiphilic Homopolymers: Synthesis, Morphology Studies and Biomedical Applications. *Chem. Commun.* **2015**, *51*, 11541–11555.
- (8) Changez, M.; Kang, N. G.; Lee, C. H.; Lee, J. S. Reversible and pH-Sensitive Vesicles from Amphiphilic Homopolymer Poly(2-(4-vinylphenyl)pyridine). *Small* **2010**, *6*, 63–68.
- (9) Wang, Y.; Alb, A. M.; He, J.; Grayson, S. M. Neutral Linear Amphiphilic Homopolymers Prepared by Atom Transfer Radical Polymerization. *Polym. Chem.* **2014**, *5*, 622–629.
- (10) Savariar, E. N.; Aathimanikandan, S. V.; Thayumanavan, S. Supramolecular Assemblies from Amphiphilic Homopolymers: Testing the Scope. *J. Am. Chem. Soc.* **2006**, *128*, 16224–16230.
- (11) Zhu, Y.; Liu, L.; Du, J. Probing into Homopolymer Self-Assembly: How Does Hydrogen Bonding Influence Morphology? *Macromolecules* **2013**, *46*, 194–203.
- (12) Mane, S. R.; Rao, N. V.; Chaterjee, K.; Dinda, H.; Nag, S.; Kishore, A.; Sarma, J. D.; Shunmugam, R. Amphiphilic Homopolymer Vesicles as Unique Nano-Carriers for Cancer Therapy. *Macromolecules* **2012**, *45*, 8037–8042.
- (13) Zhang, J.; You, S.; Yan, S.; Müllen, K.; Yang, W.; Yin, M. pH-Responsive Self-Assembly of Fluorophore-Ended Homopolymers. *Chem. Commun.* **2014**, *50*, 7511–7513.
- (14) Liu, T.; Tian, W.; Zhu, Y.; Bai, Y.; Yan, H.; Du, J. How Does a Tiny Terminal Alkynyl End Group Drive Fully Hydrophilic Homopolymers to Self-Assemble Into Multicompartment Vesicles and Flower-Like Complex Particles? *Polym. Chem.* **2014**, *5*, 5077–5088
- (15) Du, J.; Willcock, H.; Patterson, J. P.; Portman, I.; O'Reilly, R. K. Self-Assembly of Hydrophilic Homopolymers: A Matter of RAFT End Groups. *Small* **2011**, *7*, 2070–2080.
- (16) Patterson, J. P.; Kelley, E. G.; Murphy, R. P.; Moughton, A. O.; Robin, M. P.; Lu, A.; Colombani, O.; Chassenieux, C.; Cheung, D.; Sullivan, M. O.; Epps, T. H., III; O'Reilly, R. K. Structural Characterization of Amphiphilic Homopolymer Micelles Using Light Scattering, SANS, and Cryo-TEM. *Macromolecules* 2013, 46, 6319–6325.
- (17) Xu, J.; Tao, L.; Boyer, C.; Lowe, A. B.; Davis, T. P. Facile Access to Polymeric Vesicular Nanostructures: Remarkable ω-End group Effects in Cholesterol and Pyrene Functional (Co)Polymers. *Macromolecules* **2011**, *44*, 299–312.
- (18) Ramireddy, R. R.; Prasad, P.; Finne, A.; Thayumanavan, S. Zwitterionic Amphiphilic Homopolymer Assemblies. *Polym. Chem.* **2015**, *6*, 6083–6087.
- (19) He, H.; Liu, B.; Wang, M.; Vacheta, R. W.; Thayumanavan, S. Sequential Nucleophilic "Click" Reactions for Functional Amphiphilic Homopolymers. *Polym. Chem.* **2019**, *10*, 187–193.
- (20) Sun, H.; Fan, L.; Zou, K.; Zhu, H.; Du, J. Decoration of Homopolymer Vesicles by Antibacterial Ultrafine Silver Nanoparticles. *RSC Adv.* **2014**, *4*, 41331–41335.
- (21) Mabire, A. B.; Robin, M. P.; Willcock, H.; Pitto-Barry, A.; Kirby, N.; O'Reilly, R. K. Dual Effect of Thiol Addition on Fluorescent Polymeric Micelles: ON-to-OFF Emissive Switch and Morphology Transition. *Chem. Commun.* **2014**, *50*, 11492–11495.

- (22) Mane, S. R.; Rao, N. V.; Shunmugam, R. Reversible pH- and Lipid-Sensitive Vesicles from Amphiphilic Norbornene-Derived Thiobarbiturate Homopolymers. ACS Macro Lett. 2012, 1, 482–488.
- (23) Kubo, T.; Easterling, C. P.; Olsona, R. A.; Sumerlin, B. S. Synthesis of Multifunctional Homopolymers *via* Sequential Post-Polymerization Reactions. *Polym. Chem.* **2017**, *8*, 6028–6032.
- (24) Mabire, A. B.; Brouard, Q.; Pitto-Barry, A.; Williams, R. J.; Willcock, H.; Kirby, N.; Chapman, E.; O'Reilly, R. K. CO₂/pH-Responsive Particles with Built-In Fluorescence Read-Out. *Polym. Chem.* **2016**, *7*, 5943–5948.
- (25) Hu, Z.; Jonas, A. M.; Varshney, S. K.; Gohy, J. F. Dilution-Induced Spheres-to-Vesicles Morphological Transition in Micelles from Block Copolymer/Surfactant Complexes. *J. Am. Chem. Soc.* **2005**, 127, 6526–6527.
- (26) Zhang, Q.; Lei, L.; Zhu, S. Gas-Responsive Polymers. *ACS Macro Lett.* **2017**, *6*, 515–522.
- (27) Coumes, C.; Woisel, P.; Fournier, D. Facile Access to Multistimuli-Responsive Self-Assembled Block Copolymers *via* a Catechol/Boronic Acid Ligation. *Macromolecules* **2016**, *49*, 8925–8932.
- (28) Herzberger, J.; Fischer, K.; Leibig, D.; Bros, M.; Thiermann, R.; Frey, H. Oxidation-Responsive and "Clickable" Poly(ethylene glycol) via Copolymerization of 2-(Methylthio)ethyl Glycidyl Ether. J. Am. Chem. Soc. 2016, 138, 9212–9223.
- (29) Liu, X.; Zhu, J.; Ouyang, K.; Yan, Q. Peroxynitrite-Biosignal-Responsive Polymer Micelles as Intracellular Hypersensitive Nanoprobes. *Polym. Chem.* **2018**, *9*, 5075–5079.
- (30) Zhao, J.; Wang, H.; Liu, J.; Deng, L.; Liu, J.; Dong, A.; Zhang, J. Comb-like Amphiphilic Copolymers Bearing Acetal-Functionalized Backbones with the Ability of Acid-Triggered Hydrophobic-to-Hydrophilic Transition as Effective Nanocarriers for Intracellular Release of Curcumin. *Biomacromolecules* 2013, 14, 3973—3984.
- (31) Roy, D.; Brooks, W. L. A.; Sumerlin, B. S. New Directions in Thermoresponsive Polymers. *Chem. Soc. Rev.* **2013**, 42, 7214–7243.
- (32) Han, D.; Tong, X.; Zhao, Y. Block Copolymer Micelles with Dual-Stimuli-Responsive Core for Fast or Slow Degradation. *Langmuir* **2012**, 28, 2327–2331.
- (33) Wang, H.; Tang, L.; Tu, C.; Song, Z.; Yin, Q.; Yin, L.; Zhang, Z.; Cheng, J. Redox-Responsive, Core-Cross-Linked Micelles Capable of On-Demand, Concurrent Drug Release and Structure Disassembly. *Biomacromolecules* **2013**, *14*, 3706–3712.
- (34) Schattling, P.; Jochuma, F. D.; Theato, P. Multi-Stimuli Responsive Polymers the All-in-One Talents. *Polym. Chem.* **2014**, *5*, 25–36.
- (35) Jazani, A. M.; Arezi, N.; Maruya-Li, K.; Jung, S.; Oh, J. K. Facile Strategies to Synthesize Dual Location Dual Acidic pH/Reduction-Responsive Degradable Block Copolymers Bearing Acetal/Disulfide Block Junctions and Disulfide Pendants. ACS Omega 2018, 3, 8980—8001
- (36) Percec, V.; Guliashvili, T.; Ladislaw, J. S.; Wistrand, A.; Stjerndahl, A.; Sienkowska, M. J.; Monteiro, M. J.; Sahoo, S. Ultrafast Synthesis of Ultrahigh Molar Mass Polymers by Metal-Catalyzed Living Radical Polymerization of Acrylates, Methacrylates, and Vinyl Chloride Mediated by SET at 25 °C. J. Am. Chem. Soc. 2006, 128, 14156–14165.
- (37) Lligadas, G.; Grama, S.; Percec, V. Single-Electron Transfer Living Radical Polymerization Platform to Practice, Develop and Invent. *Biomacromolecules* **2017**, *18*, 2981–3008.
- (38) Anastasaki, A.; Nikolaou, V.; Haddleton, D. M. Cu(0)-Mediated Living Radical Polymerization: Recent Highlights and Applications: a Perspective. *Polym. Chem.* **2016**, *7*, 1002–1026.
- (39) Moreno, A.; Ronda, J. C.; Cádiz, V.; Galià, M.; Lligadas, G.; Percec, V. pH-Responsive Micellar Nanoassemblies from Water-Soluble Telechelic Homopolymers Endcoding Acid-Labile Middle-Chain Groups in Their Hydrophobic Sequence-Defined Initiator Residue. ACS Macro Lett. 2019, 8, 1200–1208.
- (40) Moreno, A.; Ronda, J. C.; Cádiz, V.; Galià, M.; Percec, V.; Lligadas, G. Programmed Self-Assembly and Stimuli-Triggered Response of Hydrophilic Telechelic Polymers with Sequence-Encoded Hydrophobic Initiators. *Macromolecules* **2020**, *53*, 7285–7297.

- (41) Delplace, V.; Nicolas, J. Degradable Vinyl Polymers for Biomedical Applications. *Nat. Chem.* **2015**, *7*, 771–784.
- (42) Moreno, A.; Ronda, J. C.; Cádiz, V.; Galià, M.; Lligadas, G.; Percec, V. SET-LRP from Programmed Difunctional Initiators Encoded with Double Single-Cleavage and Double Dual-Cleavage Groups. *Biomacromolecules* **2019**, *20*, 3200–3210.
- (43) Jazani, A. M.; Oh, J. K. Dual Location, Dual Acidic pH/Reduction-Responsive Degradable Block Copolymer: Synthesis and Investigation of Ketal Linkage Instability under ATRP Conditions. *Macromolecules* **2017**, *50*, 9427–9436.
- (44) Du, J.; Choi, B.; Liu, Y.; Feng, A.; Thang, S. H. Degradable pH and Redox Dual Responsive Nanoparticles for Efficient Covalent Drug Delivery. *Polym. Chem.* **2019**, *10*, 1291–1298.
- (45) Li, D.; Bu, Y.; Zhang, L.; Wang, X.; Yang, Y.; Zhuang, Y.; Yang, F.; Shen, H.; Wu, D. Facile Construction of pH- And Redox-Responsive Micelles From a Biodegradable $Poly(\beta-hydroxyl Amine)$ for Drug Delivery. *Biomacromolecules* **2016**, *1*, 291–300.
- (46) Yin, Y.; Huang, X.; Lv, C.; Wang, L.; Yu, S.; Luo, Q.; Xu, J.; Liu, J. Construction of an Artificial Glutathione Peroxidase Active Site on Copolymer Vesicles. *Macromol. Biosci.* **2010**, *10*, 1505–1516.
- (47) Syrett, J. A.; Jones, M. W.; Haddleton, D. M. A Facile Route to End-Functionalised Polymers Synthesised by SET-LRP *via* a One-Pot Reduction/Thiol-ene Michael-Type Addition. *Chem. Commun.* **2010**, 46, 7181–7183.
- (48) Rosen, B. M.; Jiang, X.; Wilson, C. J.; Nguyen, N. H.; Monteiro, M. J.; Percec, V. The Disproportionation of Cu(I)X Mediated by Ligand and Solvent into Cu(0) and $Cu(II)X_2$ and its Implications for SET-LRP. J. Polym. Sci., Part A Polym. Chem. **2009**, 47, 5606–5628.
- (49) Gillies, E. R.; Jonsson, T. B.; Fréchet, J. M. J. Stimuli-Responsive Supramolecular Assemblies of Linear-Dendritic Copolymers. *J. Am. Chem. Soc.* **2004**, *126*, 11936–11943.
- (50) Zhang, L.; Eisenberg, A. Multiple Morphologies of "Crew-Cut" Aggregates of Polystyrene-b-poly(acrylic acid) Block Copolymers. *Science* **1995**, 268, 1728–1731.
- (51) Zhang, L.; Eisenberg, A. Multiple Morphologies and Characteristics of "Crew-Cut" Micelle-like Aggregates of Polystyrene-b-poly-(acrylic acid) Diblock Copolymers in Aqueous Solutions. *J. Am. Chem. Soc.* **1996**. *118*. 3168–3181.
- (52) Mai, Y.; Zhou, Y.; Yan, D. Synthesis and Size-Controllable Self-Assembly of a Novel Amphiphilic Hyperbranched Multiarm Copolyether. *Macromolecules* **2005**, *38*, 8679–8686.
- (53) Qi, M.; Zhou, Y. Multimicelle Aggregate Mechanism for Spherical Multimolecular Micelles: from Theories, Characteristics and Properties to Applications. *Mater. Chem. Front.* **2019**, *3*, 1994–2009
- (54) Yao, Y.; Li, C.; Liu, F.; Zhao, P.; Gu, Z.; Zhang, S. Covalent Capture of Supramolecular Species in an Aqueous Solution of Water-Miscible Small Organic Molecules. *Phys. Chem. Chem. Phys.* **2019**, *21*, 10477–10487.
- (55) Ratke, L.; Voorhees, P. W.. Growth and Coarsening: Ost-Wald Ripening in Material Processing, Springer Science & Business Media, 2013
- (56) Cameron, N. S.; Corbierre, M. K.; Eisenberg, A. Asymmetric Amphiphilic Block Copolymers in Solution: a Morphological Wonderland. *Can. J. Chem.* **1999**, *77*, 1311–1326.
- (57) Li, C.; Madsen, J.; Armes, S. P.; Lewis, A. L. A New Class of Biochemically Degradable, Stimulus-Responsive Triblock Copolymer Gelators. *Angew. Chem., Int. Ed.* **2006**, *45*, 3510–3513.
- (58) Cheng, X.; Jin, Y.; Fan, B.; Qi, R.; Li, H.; Fan, W. Self-Assembly of Polyurethane Phosphate Ester with Phospholipid-Like Structures: Spherical, Worm-Like Micelles, Vesicles, and Large Compound Vesicles. ACS Macro Lett. 2016, 5, 238–243.
- (59) Liu, B.; Thayumanavan, S. Substituent Effects on the pH Sensitivity of Acetals and Ketals and Their Correlation with Encapsulation Stability in Polymeric Nanogels. *J. Am. Chem. Soc.* **2017**, *139*, 2306–2317.
- (60) Gupta, S. C.; Patchva, S.; Aggarwal, B. B. Therapeutic Roles of Curcumine: Lessons Learned from Clinical Trials. *AAPS J.* **2013**, *15*, 195–218.

- (61) Saheb, M.; Fereydouni, N.; Nemati, S.; Barreto, G. E.; Johnston, T. P.; Sahebkar, A. Chitosan-based Delivery Systems for Curcumin: A Review of Pharmacodynamic and Pharmacokinetic Aspects. *J. Cell. Physiol.* **2019**, 234, 12325–12340.
- (62) Salem, M.; Rohani, S.; Gillies, E. R. Curcumin, a Promising Anti-Cancer Therapeutic: a Review of its Chemical Properties, Bioactivity and Approaches to Cancer Cell Delivery. *RSC Adv.* **2014**, *4*, 10815–10829.
- (63) Qiao, Z.; Liu, H. Y.; Zha, J. C.; Mao, X. X.; Yin, J. Completely Degradable Backbone-Type Hydrogen Peroxide Responsive Curcumin Copolymer: Synthesis and Synergistic Anticancer Investigation. *Polym. Chem.* **2019**, *10*, 4305–4313.
- (64) Raveendran, R.; Mullen, K. M.; Wellard, R. M.; Sharma, C. P.; Hoogenboom, R.; Dargaville, T. R. Poly(2-oxazoline) Block Copolymer Nanoparticles for Curcumin Loading and Delivery to Cancer Cells. *Eur. Polym. J.* **2017**, *93*, 682–694.
- (65) Yin, Q.; Shen, J.; Zhang, Z.; Yu, H.; Li, Y. Reversal of Multidrug Resistance by Stimuli-Responsive Drug Delivery Systems for Therapy of Tumor. *Adv. Drug Delivery Rev.* **2013**, *65*, 1699–1715.
- (66) Ghosh, M.; Ryan, R. O. Curcumin Homing to the Nucleolus: Mechanism for Initiation of an Apoptotic Program. *J. Nutr. Biochem.* **2014**, 25, 1117–1123.
- (67) Miura, Y. Synthesis and Biological Application of Glycopolymers. *J. Polym. Sci., Part A: Polym. Chem.* **2007**, *45*, 5031–5036.
- (68) Bensabeh, N.; Moreno, A.; Roig, A.; Rahimzadeh, M.; Rahimi, K.; Ronda, J. C.; Cádiz, V.; Galià, M.; Percec, V.; Rodriguez-Emmenegger, C.; Lligadas, G. Photoinduced Upgrading of Lactic Acid-Based Solvents to Block Copolymer Surfactants. ACS Sustainable Chem. Eng. 2020, 8, 1276–1284.
- (69) Rosen, B. M.; Lligadas, G.; Hahn, C.; Percec, V. Synthesis of Dendritic Macromolecules through Divergent Iterative Thio-Bromo "Click" Chemistry and SET-LRP. J. Polym. Sci., Part A: Polym. Chem. **2009**, 47, 3940–3948.
- (70) Soeriyadi, A. H.; Boyer, C.; Nyström, F.; Zetterlund, P. B.; Whittaker, M. R. High-Order Multiblock Copolymers *via* Iterative Cu(0)-Mediated Radical Polymerizations (SET-LRP): Toward Biological Precision. *J. Am. Chem. Soc.* **2011**, *133*, 11128–11131.
- (71) Beyer, V. P.; Cattoz, B.; Strong, A.; Phillips, D. J.; Schwarz, A.; Becer, C. R. Fast Track Access to Multi-Block Copolymers *via* Thiol-Bromo Click Reaction of Telechelic Dibromo Polymers. *Polym. Chem.* **2019**, *10*, 4259–4270.